ROYAL SOCIETY
OF CHEMISTRY

PAPER

Check for updates

Efficient heterogeneous catalysis by pendant metalloporphyrin-functionalized polythiophenes for the electrochemical reduction of carbon dioxide†

Supranee Watpathomsub,[a] Jirapong Luangchaiyaporn,[a] Niyazi Serdar Sariciftci [ID][b] and Patchanita Thamyongkit [ID] *[a]

In this work, two novel Zn^{II}- and Co^{II}-porphyrin monomers with thiophene-based units attached *via* flexible 1,3-aminothiopropylene linkers were successfully synthesized and fully characterized. Electropolymerization of these monomers was performed on indium tin oxide (ITO)-coated glass and carbon paper *via* cyclic voltammetry (CV) to obtain the corresponding polymer films for photophysical characterization and investigation of their catalytic activities for the electrochemical reduction (ECR) of carbon dioxide (CO_2), respectively. CV and controlled potential electrolysis (CPE) in a 0.5 M $KHCO_3$ aqueous solution showed that the Zn^{II}-porphyrin-based polymer mainly supports hydrogen (H_2) evolution from water splitting, while the Co^{II}-porphyrin-based polymer predominately promotes the formation of carbon monoxide (CO). At a reduction potential of -0.66 V *vs.* reversible hydrogen electrode (RHE), equivalent to an overpotential of -0.54 V, CPE under the catalysis of the Co^{II}-porphyrin-based polymer could efficiently convert CO_2 to CO with the optimum faradaic efficiency, turnover number (TON) and turnover frequency (TOF) of 66%, 5.7×10^2 and 1.6 s^{-1}, respectively, after 1 h. The 6 h CPE suggests satisfactory film stability and steady production of CO from the ECR of CO_2, indicating the potential use of this polymer film for the reduction of CO_2 at a low overpotential under ambient conditions in aqueous media.

Introduction

In the recent decades, the increasing carbon dioxide (CO_2) emission in the atmosphere has become a serious environmental concern and threat to the global climate.[1] Accordingly, the two major approaches currently proposed for reducing the amount of CO_2 are capture and storage,[2] and CO_2 conversion and utilization.[3] The former includes capturing and then sequestrating CO_2 underground without transforming CO_2,[4] whereas the latter involves transforming CO_2 into various useful chemicals, such as carbon monoxide (CO), formic acid (HCOOH), formaldehyde (HCOH), methanol (CH_3OH) and methane (CH_4).[5–7] One of the most popular CO_2 conversion techniques is electrochemical reduction (ECR), which offers many advantages, *e.g.* possibility for heterogeneous catalysis

under mild conditions in simple compact electrochemical setups, ability to optimize and control the formation of products by varying the type of electrode and applied potential, and compatibility with several sources of alternative energy.[8] However, due to the high stability of CO_2, the direct one-electron ECR of CO_2 requires a high reduction potential (E_{red}), *i.e.* -1.90 V *vs.* normal hydrogen electrode (NHE).[9] Therefore, the development of electrocatalysts and photoelectrocatalysts to reduce CO_2 at a low E_{red} with the minimum overpotential has become of great interest.

Owing to their favorable photophysical and electrochemical properties, porphyrin and metalloporphyrin derivatives are widely known as promising materials for electronic and optoelectronic applications, such as organic light-emitting diodes (OLEDs),[10–14] organic field-effect transistors (OFETs),[15–18] dye-sensitized solar cells (DSSCs),[19–24] and bulk heterojunction solar cells (BHJSCs).[21,25–27] Furthermore, the possibilities for their structural modification by introducing various central metals and peripheral substituents enable these photophysical and electrochemical properties to be enhanced. Although there are many reports describing the use of metalloporphyrins for the ECR of CO_2, most derivatives still encounter limited charge

[a] *Department of Chemistry, Faculty of Science, Chulalongkorn University, Bangkok 10330, Thailand. E-mail: patchanita.v@chula.ac.th*

[b] *Linz Institute for Organic Solar Cells (LIOS), Institute of Physical Chemistry, Johannes Kepler University, Linz 4040, Austria*

† Electronic supplementary information (ESI) available: Spectral data, including ^{1}H-NMR, ^{13}C-NMR, mass, absorption and emission spectra, as well as calibration curves for new compounds. See DOI: 10.1039/d0nj01381a

mobility and stability, which affect their electrocatalytic performance.[1,28–37] Some possible approaches to enhance the charge mobility of these organic materials include extension of their π-conjugation systems by creating polymer networks and integrating conductive unit(s) with the porphyrin macrocycles.[38] Polythiophene is a well-known conjugated polymer owing to its high conductivity, high stability and advantageous electrochemical properties.[39] Moreover, its photophysical, electrochemical and electronic properties can be tuned by modifying the substituents at the α- and β-positions of its thiophene rings.[40] Several studies have reported the incorporation of porphyrins and conductive polymers for applications such as chemical sensing,[41] photoelectrochemical conversion,[17,42–45] and electrocatalysis.[41,46,47] However, although chemical polymerization is a popular method for preparing large polymer chains of a wide range of thiophene monomeric derivatives, electropolymerization offers several advantages over the chemical approach. This method allows direct grafting of the polymer onto many types of substrates with a controllable film thickness and the possibility for *in situ* characterization during the polymer growth process *via* various electrochemical and/or spectroscopic techniques, and does not require the use of catalysts and complicated purification steps.[48,49]

In this research, we focused on the synthesis and characterization of the photophysical and electrochemical properties of novel polythiophenes functionalized with pendant metalloporphyrin units. The molecular structure of each monomer consists of a Zn- or Co-metallated *meso*-substituted porphyrin ring with a thiophene (**T**)-3,4-ethylenedioxythiophene (**EDOT**) moiety attached *via* a flexible 1,3-aminothiopropylene spacer (Fig. 1). We exploited the benefits of the readily electropolymerizable **T-EDOT** precursor reported by Roncali *et al.*[50] for the preparation of a conductive polymeric support, which provided a flexible bridge to bring the porphyrin electrocatalysts in proximity to the electrodes for the efficient ECR of CO$_2$.

Results and discussion

Synthesis

The synthesis of the target porphyrins started from the alkylation of compound **2**[51] with 1,3-dibromopropane in the presence
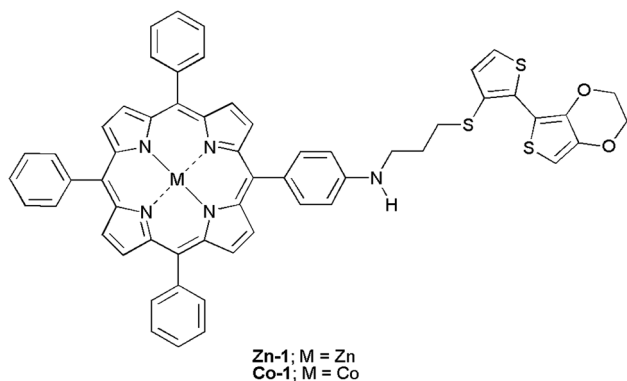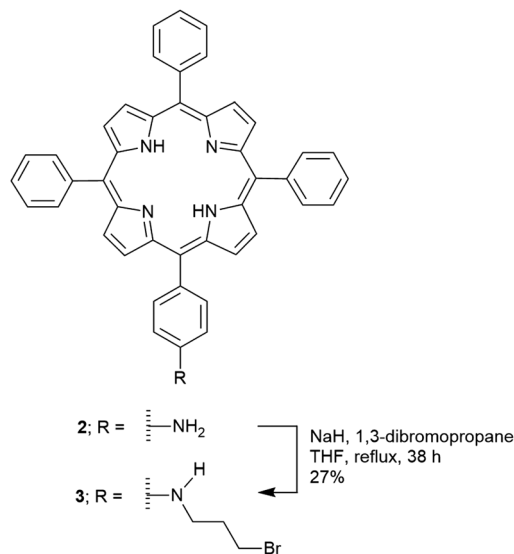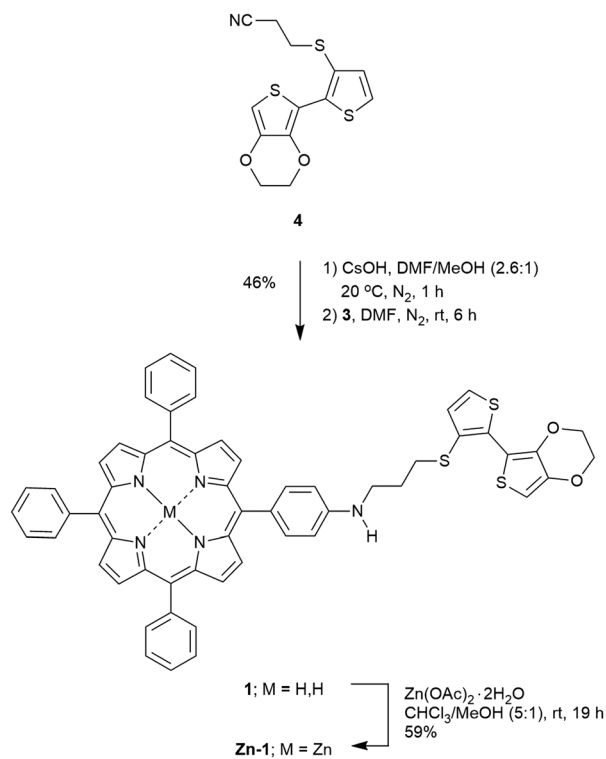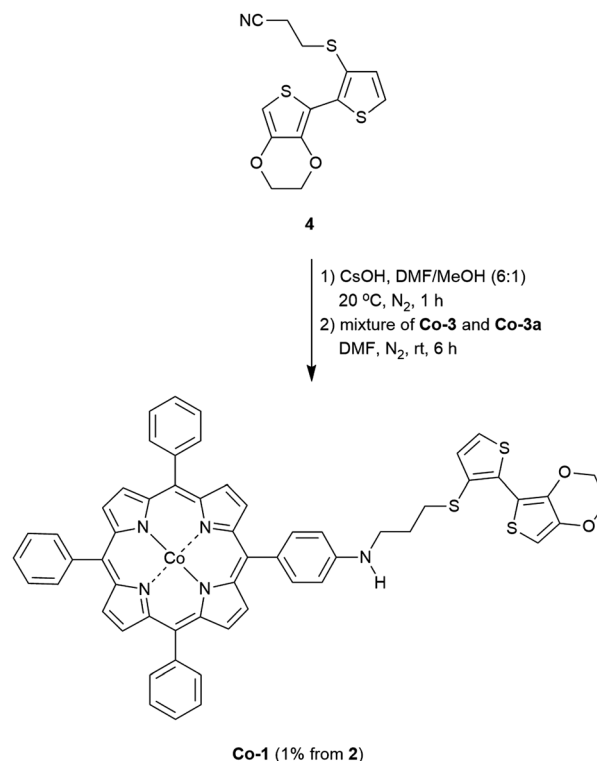

Scheme 1 Synthesis of precursor **3**.

of NaH in refluxing THF for 38 h,[52] resulting in compound **3** in 27% yield (Scheme 1). According to mass spectroscopy (MS) and thin-layer chromatography (TLC), the low yield of compound **3** is attributed to the concurrent formation of dialkylated and elimination products, which were difficult to remove by column chromatography. The successful formation of compound **3** was confirmed by [1]H-nuclear magnetic resonance spectroscopy (^{1}H-NMR), showing the characteristic inner proton peak of the free base porphyrin at −2.69 ppm, 3 multiplet signals, indicating 6 protons of an *N*-alkyl chain at 2.28–3.71 ppm, and a signal of an amino proton at 3.98–4.05 ppm (Fig. S1, ESI†). Furthermore, matrix-assisted laser desorption ionization mass spectrometry (MALDI-TOF-MS) exhibited its $[M]^+$ peak at m/z 750.794 (Fig. S3, ESI†).

To obtain compound **Zn-1**, the deprotection of a thiolate group of compound **4**[50] by cesium hydroxide[50] and subsequent treatment with compound **3** at room temperature for 6 h led to compound **1** in 46% yield (Scheme 2). The ^{1}H-NMR spectrum of compound **1** showed the characteristic singlet peak of the inner N–H protons of the free base porphyrin at −2.72 ppm and multiplet peaks of the newly introduced propylene protons at 1.98–3.52 ppm (Fig. S6, ESI†). Moreover, a new broad singlet peak of an N–H proton at 4.01 ppm and multiplet signals indicating ethylene protons of the **EDOT** unit at 4.18–4.42 ppm were also observed. Its high-resolution electrospray ionization (HR-ESI) mass spectrum exhibited a molecular ion peak at m/z 926.2652, reaffirming the successful formation of compound **1** (Fig. S8, ESI†). The absorption spectrum of compound **1** exhibited a Soret band at 422 nm, and Q-bands at 518, 555, 594 and 651 nm (Fig. S9, ESI†). Upon excitation at its absorption maximum, the typical emission peaks of the freebase porphyrin at 653 and 719 nm were observed (Fig. S11, ESI†). Metallation of **1** with Zn(OAc)$_2$·2H$_2$O was performed at room temperature for 19 h,[53] resulting in **Zn-1** in 59% yield. Disappearance of the singlet peak at −2.72 ppm in the ^{1}H-NMR spectrum (Fig. S12, ESI†) and the emission peak at 719 nm

Fig. 1 Structure of the target monomers.

Published on 24 June 2020. Downloaded by Johannes Kepler Universitat Linz on 7/14/2020 9:39:17 AM.

NC
S
S
S
O
O
4
46%
1) CsOH, DMF/MeOH (2.6:1)
20 °C, N2, 1 h
2) 3, DMF, N2, rt, 6 h
N
N
M
N
N
S
O
O
S
S
N
H
1; M = H,H
Zn(OAc)2·2H2O
CHCl3/MeOH (5:1), rt, 19 h
59%
Zn-1; M = Zn

Scheme 2 Synthesis of compound **Zn-1**.

NC
S
S
S
O
O
4
1) CsOH, DMF/MeOH (6:1)
20 °C, N2, 1 h
2) mixture of Co-3 and Co-3a
DMF, N2, rt, 6 h
N
N
Co
N
N
S
O
O
S
S
N
H
Co-1 (1% from 2)

Scheme 3 Synthesis of compound **Co-1**.

(Fig. S17, ESI†), which were observed for compound **1**, indicated completion of the Zn-metallation process. The HR-ESI mass spectrum of **Zn-1** showed a molecular ion peak at *m*/*z* 988.1792 and $[M - Zn]^+$ peak at *m*/*z* 926.2661 (Fig. S14, ESI†). Its absorption spectrum exhibited a Soret band at 429 nm, and Q-bands at 555 and 605 nm (Fig. 2 and Fig. S15, ESI†). Excitation of **Zn-1** at its absorption maximum gave emission peaks at 613 and 657 nm (Fig. S17, ESI†).

Due to the difficulties in separating compound **3** from the elimination by-product, the crude product containing compound **3** was directly used for Co-metallation with $Co(OAc)_2{\cdot}4H_2O$ in a similar manner as the above-described Zn-metallation to obtain a mixture containing **Co-3**.[54] The disappearance of the emission peak at 719 nm observed for compound **1** indicated completion of the Co-metallation process. The resulting crude containing **Co-3** was further coupled with the **T-EDOT** unit under the same conditions as that performed for preparing **Zn-1** (Scheme 3). After chromatographic purification, compound **Co-1** was purely separated and its formation was confirmed by the molecular ion peak in its HR-ESI mass spectrum at *m*/*z* 982.1758 (Fig. S18, ESI†). The UV-visible absorption spectrum of **Co-1** exhibited a characteristic Soret band at 432 nm, and Q-bands at 550 and 596 nm, as shown in Fig. 2 and Fig. S19 (ESI†). Upon excitation at its absorption maximum, **Co-1** showed emission peaks at 611 and 656 nm (Fig. S21, ESI†).

(a)
429
438
Zn-1 solution
poly(Zn-1)/ITO
564
608
555
605
(b)
432
442
Co-1 solution
poly(Co-1)/ITO
550
600
550
596
Absorbance
1.0
0.8
0.6
0.4
0.2
0.0
0.5
0.4
0.3
0.2
0.1
0.0
300
400
500
600
700
800
Wavelength / nm

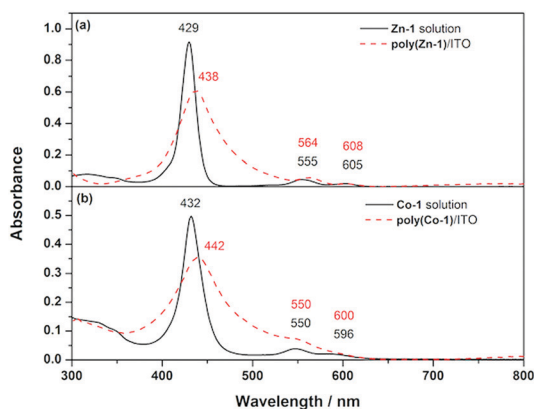

Fig. 2 Absorption spectra of monomer solutions in toluene (black solid line) and polymer films (red dashed line) of (a) **Zn-1** and (b) **Co-1** on ITO-coated glass.

Electrochemical polymerization of the target monomers

Polymer films of **Zn-1** and **Co-1** were prepared *via* electropolymerization on indium-tin-oxide (ITO)-coated glass and carbon paper substrates. ITO-coated glass was used as the substrate to develop optimized electropolymerization conditions for both target monomers, and their transparency enabled comparison of the absorption profiles of the resulting polymer films with that of their monomer solutions. The major purpose of using carbon paper as a substrate was to increase the surface area of the polymer films, which should lead to enhanced productivity in the ECR of CO_2.[55] Electropolymerization was carried out in a one-compartment three-electrode electrochemical setup consisting of the ITO-coated glass or the carbon paper as the working electrode (WE), Pt plate as the counter electrode (CE) and a silver chloride-coated silver

wire quasi-reference electrode (Ag/AgCl QRE). All the potentials against the Ag/AgCl QRE were calibrated with the formal potential (E^0) of a ferrocen-ium/ferrocene (Fc$^+$/Fc) redox couple as an external standard and converted to the NHE scale.[56] Oxidation potentials (E_{ox}) ranging from 0.36 V to 1.96 V vs. NHE and from 0.36 V to 2.06 V vs. NHE were applied to the electrochemical cell when the ITO-coated glass and carbon paper were used, respectively, at a scan rate of 50 mV s^{-1} for 10 scanning cycles.

As shown in Fig. 3a, the cyclic voltammograms obtained from the electropolymerization of **Zn-1** on ITO-coated glass showed reversible metalloporphyrin ring oxidation at peak potentials (E_{peak}) of 1.22 V and 1.46 V vs. NHE,[57–60] and a quasi-reversible peak corresponding to the formation of polythiophene at 1.78 V vs. NHE in the first scanning cycle.[61] With an increase in the number of scanning cycles, an increase in the peak current and slight positive potential shift of the oxidation peaks were observed, indicating the undergoing polymerization on the electrode. The polymerization of **Zn-1** on carbon paper gave similar porphyrin ring oxidation peaks with a slightly more complex peak pattern of the **T-EDOT** oxidative polymerization at 1.78 V to 1.83 V vs. NHE compared with that observed in the case of the ITO-coated glass (Fig. 3b). This behavior is attributed to the higher degree of polymerization due to the higher electroactive surface area of the carbon paper, which was confirmed by the approximately 10-fold higher current density observed in this case compared with the polymerization on the ITO-coated glass. After the completion of the process and subsequent washing to remove the remaining monomer, the polymer films of **Zn-1** (**poly(Zn-1)**) were obtained on both substrates as brown films, which were found to be stable in the ambient atmosphere.

Similarly, the electropolymerization of **Co-1** was carried out on ITO-coated glass and carbon paper using the same potential range, scan rate and number of scanning cycles. As shown in Fig. 3c and d, reversible Co^{II}/Co^{III} and macrocycle oxidation

peaks were observed from 0.98 V to 1.03 V vs. NHE and from 1.43 V to 1.56 V vs. NHE, respectively,[41,62] while an irreversible voltammetric signal corresponding to the polymerization of **T-EDOT** was seen at the end of the potential window.[61] The irreversible profile possibly originated from charge trapping behavior, as observed previously in the electropolymerization of 2,2′-bithiophene.[63] Along the course of the electropolymerization, the peak current of these oxidation peaks was found to increase with a positive potential shift when the number of scanning cycles increased, indicating the occurring polymerization process, which led to stable brown films of the corresponding polymer, **poly(Co-1)**, on the substrates.

The cyclic voltammograms of both polymer films on the ITO-coated glass and the carbon paper recorded in a 0.1 M TBAPF$_6$ solution in DMF in the potential range of 0.36 V to 1.66 V vs. NHE showed similar patterns as that observed during the electropolymerization (Fig. 4). The metalloporphyrin ring oxidation peaks of the **poly(Zn-1)** film were observed at E_{peak} of 1.06–1.08 V and 1.24–1.46 V vs. NHE, respectively. In the case of the **poly(Co-1)** film, the Co^{II}/Co^{III} and the metalloporphyrin ring oxidation peaks were detected at E_{peak} of 1.08 V and 1.42–1.45 V vs. NHE, respectively.

According to UV-visible spectrophotometry, both the **poly(Zn-1)** and **poly(Co-1)** polymer films on the ITO-coated glass showed Soret bands at 438–442 nm, and Q bands at 550–564 nm and 600–608 nm, which are consistent with the absorption of their monomer solutions (Fig. 2). The slight red shift and peak broadening observed in the case of the polymer films are attributed to the extended conjugation systems in the polymer networks and the aggregation of the porphyrin macrocycles. This observation confirmed the presence of the Zn^{II}- and Co^{II}-porphyrin units in the networks of **poly(Zn-1)** and **poly(Co-1)**, respectively.

Electrocatalytic activities of the target polymers towards the reduction of CO$_2$

To investigate the heterogeneous ECR of CO$_2$ in the presence of the **poly(Zn-1)** and **poly(Co-1)** films, cyclic voltammetry (CV) was
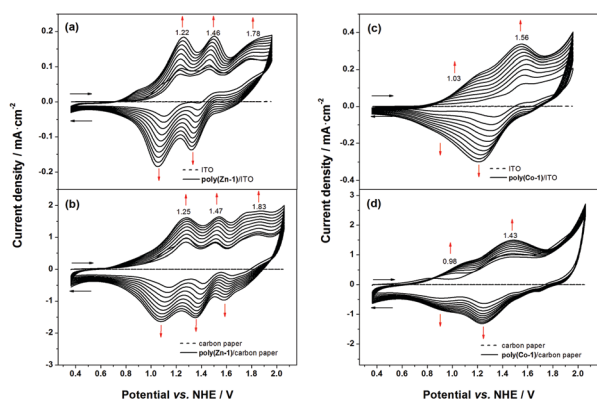

Fig. 3 Cyclic voltammograms from the electropolymerization (solid line) of (a) **Zn-1** on ITO-coated glass, (b) **Zn-1** on carbon paper, (c) **Co-1** on ITO-coated glass and (d) **Co-1** on carbon paper in comparison with that of a blank 0.1 M TBAPF$_6$ solution in CH$_2$Cl$_2$ (dashed line). The electropolymerization was performed using a 0.1 M TBAPF$_6$ solution in CH$_2$Cl$_2$ containing 0.25 mM monomer at a scan rate of 50 mV s^{-1} for 10 cycles.
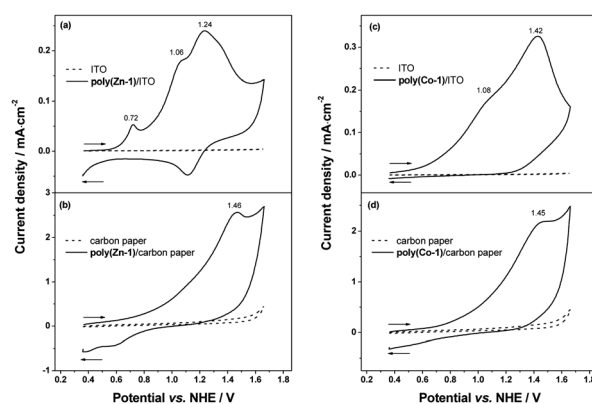

Fig. 4 Cyclic voltammograms of **poly(Zn-1)** on (a) ITO-coated glass and (b) carbon paper, and **poly(Co-1)** on (c) ITO-coated glass and (d) carbon paper (solid lines) in comparison with that of a blank 0.1 M TBAPF$_6$ solution in DMF (dashed lines). Cyclic voltammetry was performed in 0.1 M TBAPF$_6$ solution in DMF at a scan rate of 50 mV s^{-1}.

performed in a 0.5 M $KHCO_3$ aqueous solution using a three-electrode two-compartment system (H-cell) consisting of the polymer-modified carbon paper as the WE, the Pt plate as the CE and Ag/AgCl, 3 M KCl as the reference electrode (RE). The potential was swept in the range of 0.00 V to −1.30 V $vs.$ Ag/AgCl, in 3 M KCl, which is equivalent to −0.59 V and −0.66 V $vs.$ reversible hydrogen electrode (RHE),[64] under N_2- (pH 8.4) and CO_2- (pH 7.3) saturated 0.5 M $KCHO_3$ solutions, respectively. The reduction potential for the ECR of CO_2 was limited to −0.66 V $vs.$ RHE in this study to avoid significant hydrogen (H_2) formation from water splitting on the bare carbon paper surface and possible degradation of the Zn^{II}-porphyrin, as reported in a previous study.[65] The electrochemical behavior of the polymer films was studied in N_2-saturated electrolyte solutions, while their electrocatalytic activities for the ECR of CO_2 were investigated under CO_2-saturated conditions.

As shown in Fig. 5a, the cyclic voltammograms of the **poly(Zn-1)**-modified carbon paper (**poly(Zn-1)**/carbon paper) under the N_2- and CO_2-saturated conditions exhibited onset reduction potentials ($E_{red,onset}$) at −0.40 V and −0.47 V $vs.$ RHE, respectively, with a continuous increase in current density until the end of the potential window. At −0.59 V $vs.$ RHE under the CO_2-saturated condition, the current density increased to 0.95 mA cm^{-2}, which is comparable to the value of 0.92 mA cm^{-2} observed under the N_2-saturated condition. In the case of the **poly(Co-1)**-modified carbon paper (**poly(Co-1)**/carbon paper), the cyclic voltammograms under the N_2-saturated condition showed $E_{red,onset}$ at −0.46 V $vs.$ RHE (Fig. 5b). Under the CO_2-saturated condition, the cyclic voltammogram appeared to exhibit a slightly

positive shift in $E_{red,onset}$ to −0.45 V $vs.$ RHE with a large increase in the current density to 4.01 mA cm^{-2} at −0.59 V $vs.$ RHE compared with the value of 1.96 mA cm^{-2} observed under the N_2-saturated condition at the same E_{red}.

The electrochemical behavior observed in the CV experiments in the presence of the **poly(Zn-1)** and **poly(Co-1)** films led us to further investigate their catalytic performance in terms of reduction product(s) in headspace gas, especially CO and H_2, and film stability by means of controlling potential electrolysis (CPE). In this study, the constant potential of −0.66 V $vs.$ RHE was applied to the above-mentioned H-cell in the CO_2-saturated 0.5 M $KHCO_3$ solution (pH = 7.3) for 1 h and then headspace gas analysis by gas chromatography (GC) was performed. This potential represents an overpotential of −0.54 V from thermodynamic reduction of CO_2 to CO product (E^0 = −0.12 V $vs.$ RHE in 0.5 M $KHCO_3$ aqueous solution).[66] The results showed that when **poly(Zn-1)**/carbon paper was used as the WE, CO and hydrogen (H_2) were formed with faradaic efficiencies (FE)[67] of 2% and 71%, respectively (Table 1). According to the total charge integration in the CV experiments, the electrochemically active coverage of **poly(Zn-1)**/carbon paper was determined to be 1.03 × 10^{-8} mol cm^{-2}. Therefore, the turnover number (TON) and turnover frequency (TOF)[68] of the formation of the major product, $i.e.$ H_2, were found to be 7.6 × 10^2 and 0.2 s^{-1}, respectively. The sum of % FE was significantly lower than the 100% theoretical maximum, which may have resulted from the formation of other minor reduction products both in the headspace gas and liquid phase other than CO, H_2 and formate ions investigated in this work. Compared with the CPE using bare carbon paper as the WE, the % FE of H_2 formation seemed to be comparable. However, the amount of H_2 obtained from the CPE under catalysis of **poly(Zn-1)**/carbon paper was found to be approximately 1.5 times that detected in the case where bare carbon paper was used, $i.e.$ 7.77 × 10^{-6} mol $vs.$ 4.9 × 10^{-6} mol. Throughout the course of the CPE, a constant current density was observed, suggesting the steady production of H_2 catalyzed by **poly(Zn-1)**/carbon paper. To investigate the change in the **poly(Zn-1)** film after the CPE, the cyclic voltammograms of the pre- and post-electrolysis **poly(Zn-1)**/carbon
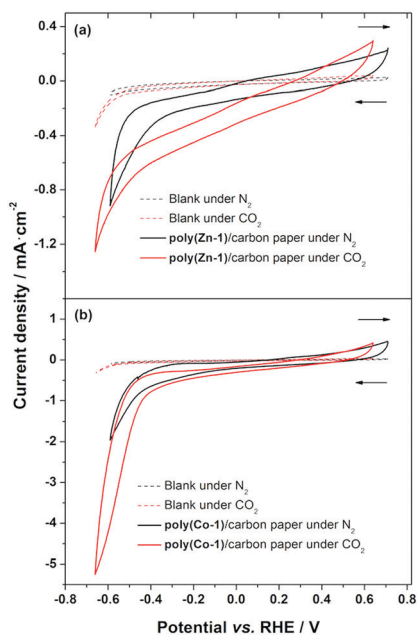

Fig. 5 Cyclic voltammograms of (a) **poly(Zn-1)**- and (b) **poly(Co-1)**-modified carbon papers under N_2- (black solid line) and CO_2- (red solid line) saturated conditions compared with that of 0.5 M $KHCO_3$ aqueous solutions under the N_2- (black dashed lines) and CO_2- (red dashed lines) saturated conditions.

Table 1 Faradaic efficiencies, TON and TOF obtained from CPE experiments under the catalysis of **poly(Zn-1)**/and **poly(Co-1)**/carbon paper

Compound/reduction time	FE/%[a]		Major product formation	
	CO	H_2	TON[b]	TOF[c]/s^{-1}
Bare carbon paper/1 h	—[d]	65	—[e]	—[e]
poly(Zn-1)/1 h	2	71	7.6 × 10^2	0.2
poly(Co-1)/1 h	66	30	5.7 × 10^3	1.6
poly(Co-1)/6 h[f]	36[g]	—[d]	1.4 × 10^{4g}	0.6[g]

[a] Faradaic efficiency (%) = [(n × N × F)/Q] × 100; when n = the number of electrons required for the reduction of CO_2 to form the product (for CO and H_2, n = 2), N = the moles of the gas product, F = Faraday's constant (96 485 C mol^{-1} of electrons) and Q = the total charge in Coulomb passed across the electrode during the electrolysis.[67] [b] TON = mol CO detected/electrochemically active surface area. [c] TOF = TON/time. [d] Product analysis was not performed. [e] Value could not be determined. [f] CPE experiment was carried out by using on-line GC analysis. [g] Average value was reported.
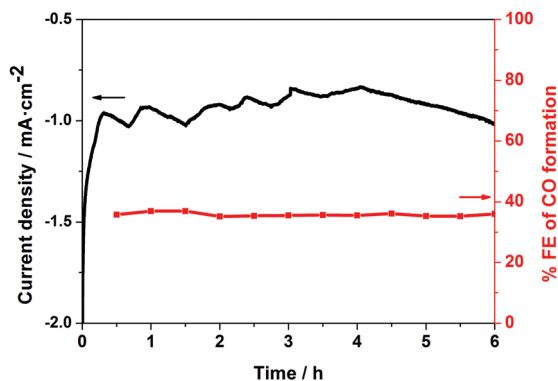
Fig. 6 Current density–time (black solid line) and % FE–time plots (square symbol with red line) of 6 h CPE using **poly(Co-1)**/carbon paper as the WE in CO_2-saturated 0.5 M $KHCO_3$ aqueous solution at applied potentials of −0.66 V vs. RHE.

paper samples were investigated in 0.1 M $TBAPF_6$ solution in DMF and compared (Fig. S22, ESI†). Upon 1 h CPE under the CO_2-saturated condition, the first ligand reduction peak was negatively shifted from −0.93 V to −1.20 V vs. NHE. This is attributed to the carboxylation of the porphyrin macrocycle, as described in previous reports, leading to an intermediate species that was inactive for the ECR of CO_2 but still catalyzed the competitive water splitting.[69–72] Consequently, **poly(Zn-1)**/carbon paper led to the selective and efficient catalysis of for the evolution of H_2 from water rather than the ECR of CO_2, as expected. This observation is consistent with a previous report describing that the formation of H_2 was dominant in a Zn^{II}-porphyrin-based electrocatalytic system, unless a high E_{red} was used.[34]

The CPE in the presence of **poly(Co-1)** gave CO and H_2 in 66% and 30% FE, respectively, after 1 h. In a similar manner to the case of **poly(Zn-1)**/carbon paper, the electrochemically active coverage of **poly(Co-1)**/carbon paper was obtained from the total charge integration and found to be 2.71×10^{-9} mol cm^{-2}. Therefore, the TON and TOF of the formation of CO as the major product was determined to be 5.7×10^3 and 1.6 s^{-1}, respectively. The H_2 evolution detected in this case possibly resulted from the partial exposure of the bare carbon paper surface on the **poly(Co-1)**/carbon paper electrode. Upon extension of the electrolysis time to 6 h, the current densities were relatively steady throughout the experiment with the average value of 0.936 mA cm^{-2} (Fig. 6). Reaction monitoring by on-line GC of a headspace gas sample every 30 min showed the average % FE of 36 with an accumulated amount of CO, TON and TOF of 0.92 mL, 1.4×10^4 and 0.6 s^{-1}, respectively (Table S1, ESI†). The change in the current density observed during the CPE resulted from the formation of Co^I-based intermediate(s), as previously described by Hu et al.[73] and some other unknown electrochemically active species. According to the CV measurements in 0.1 M $TBAPF_6$ solution in DMF, the pre- and post-electrolysis **poly(Co-1)** films gave consistent cyclic voltammogram patterns due to the persistence of the pristine **poly(Co-1)** (Fig. S23, ESI†). However, the decrease in the current density observed in the case of the post-electrolysis film is attributed to the above-mentioned irreversible formation of active intermediates,

which did not exhibit the reduction peaks in the potential range used in this study. Moreover, the inevitable detachment of the polymer from the carbon paper during the washing process, electrochemical setup preparation and N_2 purging in the post-electrolysis CV measurement were also the main reasons for the reduction in current density. Compared to the 1 h batch experiment, the lower performance values obtained in this case resulted from the difference in the electrochemical setup and the product analysis method. The 1 h CPE was performed in a closed system and the gas products were analyzed once at the end of the reaction, while the 6 h CPE was carried out in an open system with on-line product monitoring every 30 min. These results indicated satisfactory catalytic efficiency and stability of the **poly(Co-1)** film under the applied ECR condition using a relatively low overpotential, i.e. −0.54 V from the thermodynamic potential of CO_2 to CO reduction (E^0 = −0.12 V vs. RHE in 0.5 M $KHCO_3$ aqueous solution).[66] This overpotential level is comparable with that previously reported for Co^{II}-porphyrin-based covalent organic frameworks[74,75] and electrodes for the ECR of CO_2,[73,76] except that the % FE and product selectivity of **poly(Co-1)**/carbon paper still needs to be improved. However, the simple preparation method of **poly(Co-1)**/carbon paper is a competitive advantage over several reported heterogeneous Co^{II}-porphyrin-based catalysts and provides a number of opportunities to further develop the electrode performance. The superior catalytic performance of **poly(Co-1)** in terms of the formation of CO compared to **poly(Zn-1)** is attributed to the metal-centered electron transfer mechanism via strong binding between the Co^I oxidation state of the Co^{II}-porphyrin and CO_2 as mentioned above, which is more efficient than the through-ligand process proposed for the latter case.[76,77]

Conclusions

Two novel Zn^{II}- and Co^{II}-porphyrin monomers bearing the **T-EDOT** unit were synthesized and used to prepare porphyrin pendant polymers through electropolymerization. Consequently, stable homogeneous films of the corresponding polymers, **poly(Zn-1)** and **poly(Co-1)**, respectively, were readily formed on ITO-coated glass and carbon paper. The current enhancement observed in the CV studies under the CO_2-saturated condition in the presence of both polymer films on carbon paper compared with that obtained under the N_2-saturated condition indicated the catalyzed electrochemical processes caused by these polymers. The quantitative product analysis by GC and determination of the catalytic performance by CPE showed that **poly(Co-1)**/carbon paper could efficiently promote the heterogeneous ECR of CO_2 to give CO of up to 66% FE with TON and TOF of 5.7×10^3 and 1.6 s^{-1}, respectively. The **poly(Co-1)** film could well tolerate the ECR condition, giving relatively constant current densities and % FE throughout the course of the 6 hour CPE with the average values of 0.936 mA cm^{-2} and 36, respectively. However, **poly(Zn-1)** tended to favor the evolution of H_2 from water splitting rather

than the expected ECR of CO_2, and thus its use for this application will be further investigated and reported elsewhere.

Experimental

Material and methods

All chemicals were obtained from commercial suppliers and used without further purification. ^{1}H-NMR and ^{13}C-NMR spectra were recorded in deuterated chloroform ($CDCl_3$) at 400 MHz for ^{1}H and 100 MHz for ^{13}C nuclei. Chemical shifts (δ) are reported in parts per million (ppm) relative to residual $CHCl_3$ peaks (7.26 ppm and 77.2 ppm for ^{1}H- and ^{13}C-NMR spectroscopy, respectively). Mass spectra were obtained by HR-ESI-MS and MALDI-TOF-MS using dithranol as the matrix. Absorption and emission spectra were measured in toluene at room temperature and the absorption extinction coefficient (ε) is reported in $M^{-1} cm^{-1}$.

Non-commercial compounds

5-(4-Aminophenyl)-10,15,20-triphenylporphyrin (**2**)[51] and 2-(3,4-ethylenedioxy-thienyl)-3-(2-cyanoethyl-sulfanyl)-thiophene (**4**)[50] were prepared using literature procedures.

Synthesis of compound 3

Following a previously published procedure[52] with slight modification in the stoichiometric ratio of the precursors and reaction time, a solution of **2**[51] (447 mg, 0.710 mmol) in THF (35 mL) was treated with NaH (60% w/w, 117 mg, 2.92 mmol) at room temperature under an N_2 atmosphere. After 15 min, 1,3-dibromopropane (0.7 mL, 7 mmol) was added to the resulting purple suspension, and then the mixture was refluxed for additional 38 h. After the reaction was cooled to room temperature, it was quenched with a saturated aqueous solution of NH_4Cl and extracted with EtOAc. The organic phase was washed with water, dried over anhydrous $MgSO_4$ and concentrated to dryness. The resulting crude product was purified by column chromatography [silica gel, 0.1% Et_3N in CH_2Cl_2/hexanes (1:1)] to afford compound **3** as a purple solid (144 mg, 27%). ^{1}H-NMR (δ): −2.69 (s, 2H), 2.28–2.36 (m, 2H), 3.52–3.59 (m, 2H), 3.62–3.71 (m, 2H), 3.98–4.05 (m, 1H), 6.96 (d, J = 8.0 Hz, 2H), 7.71–7.83 (m, 9H), 8.03 (d, J = 8.0 Hz, 2H), 8.19–8.30 (m, 6H), 8.86 (s, 6H), 8.94–9.01 (m, 2H) (Fig. S1, ESI†); ^{13}C-NMR (δ): 31.3, 32.5, 42.5, 111.3, 119.8, 120.1, 121.2, 126.8, 127.8, 131.6, 134.7, 136.0, 142.4, 142.5, 147.7 (Fig. S2, ESI†); MALDI-TOF-MS m/z: found, 750.794 [M^+]; calcd, 750.726 (M = $C_{47}H_{36}BrN_5$) (Fig. S3, ESI†); λ_{abs} ([**3**] = 1.65 μM) 421, 520, 557, 598, 652 nm (Fig. S4, ESI†); λ_{em} (λ_{ex} = 421 nm, [**3**] = 0.55 μM) 654, 720 nm (Fig. S5, ESI†).

Synthesis of compound 1

Following a previously published procedure[50] with slight modification in the concentration of precursors, a solution of **4**[50] (45 mg, 0.14 mmol) in anhydrous DMF (2.1 mL) was cooled to 20 °C under an N_2 atmosphere. Then, a solution of CsOH (28 mg, 0.17 mmol) in degassed MeOH (0.8 mL) was added dropwise and the reaction was left to proceed at 20 °C for 1 h.

Subsequently, a solution of **3** (82 mg, 0.70 mmol) in anhydrous DMF (2.6 mL) was added at room temperature and the reaction was continued at room temperature for an additional 6 h. Then, the mixture was diluted with CH_2Cl_2, washed with water, dried over anhydrous $MgSO_4$ and concentrated to dryness. The resulting crude was purified by column chromatography [silica gel, CH_2Cl_2/hexanes (1:1)] to obtain compound **1** as a purple solid (47 mg, 46%). ^{1}H-NMR (δ): −2.72 (s, 2H), 1.98–2.15 (m, 2H), 3.02–3.10 (m, 2H), 3.39–3.52 (m, 2H), 4.01 (s, 1H), 4.18–4.26 (m, 2H), 4.26–4.42 (m, 2H), 6.43 (s, 1H), 6.91 (d, J = 8.0 Hz, 2H), 7.13 (d, J = 4.0 Hz, 1H), 7.30 (d, J = 8.0 Hz, 1H), 7.66–7.84 (m, 9H), 8.00 (d, J = 8.0 Hz, 2H), 8.16–8.31 (m, 6H), 8.84 (s, 6H), 8.92–9.01 (m, 2H) (Fig. S6, ESI†); ^{13}C-NMR (δ): 29.4, 34.4, 43.0, 64.6, 65.2, 99.9, 111.3, 119.8, 120.1, 121.4, 124.1, 126.8, 127.8, 131.2, 132.0, 134.7, 136.0, 142.4, 142.5, 147.9 (Fig. S7, ESI†); HR-ESI-MS m/z: [M + H]$^+$ calcd for $C_{57}H_{43}N_5O_2S_3$, 926.2652; found 926.2663 (Fig. S8, ESI†); UV-vis: λ_{abs} (ε, [**1**] = 2.50 μM) 422 (2.8 × 10^{5}), 518, 555, 594, 651 nm (Fig. S9 and S10, ESI†); λ_{em} (λ_{ex} = 422 nm, [**1**] = 0.27 μM) 653, 719 nm (Fig. S11, ESI†).

Synthesis of compound Zn-1

Following a previously published procedure,[53] a solution of **1** (34 mg, 0.037 mmol) in $CHCl_3$ (10.00 mL) was treated with a solution of Zn(OAc)$_2$·2H$_2$O (42 mg, 0.19 mmol) in MeOH (2.0 mL) at room temperature. After 19 h, the reaction mixture was diluted with CH_2Cl_2, and subsequently washed with water and a saturated aqueous solution of $NaHCO_3$. The organic phase was combined, dried over anhydrous $MgSO_4$ and concentrated to dryness. The crude product was purified by column chromatography [silica gel, CH_2Cl_2/hexanes (2:1)], followed by washing with hexanes and MeOH under ultrasonic agitation to obtain compound **Zn-1** as a purple solid (22 mg, 59%). ^{1}H-NMR (δ): 1.59–1.71 (m, 2H), 2.63–2.73 (m, 2H), 2.74–2.82 (m, 2H), 3.01 (s, 1H), 4.07–4.15 (m, 2H), 4.19–4.28 (m, 2H), 6.27 (s, 1H), 6.38 (d, J = 8.0 Hz, 2H), 6.96 (d, J = 4.0 Hz, 1H), 7.22 (d, J = 4.0 Hz, 1H), 7.67–7.79 (m, 9H), 7.85 (d, J = 8.0 Hz, 2H), 8.18–8.27 (m, 6H), 8.88–8.96 (m, 6H), 8.97–9.03 (m, 2H); (Fig. S12, ESI†); ^{13}C-NMR (δ): 29.9, 34.0, 64.4, 65.1, 99.8, 121.1, 124.0, 126.66, 126.73, 127.6, 127.7, 131.9, 132.0, 132.05, 132.27, 132.33, 132.5, 134.6, 135.3, 135.5, 142.9, 143.1, 143.2, 150.2, 150.3, 150.36, 150.42, 150.5, 150.6, 150.9 (Fig. S13, ESI†); HR-ESI-MS m/z: [M + H]$^+$ calcd for $C_{57}H_{41}N_5O_2S_3Zn$, 988.1787; found 988.1792 (Fig. S14, ESI†); λ_{abs} (ε, [**Zn-1**] = 1.82 μM) 429 (2.8 × 10^{5}), 555, 605 nm (Fig. S15 and S16, ESI†); λ_{em} (λ_{ex} = 430 nm, [**Zn-1**] = 0.43 μM) 613, 657 nm (Fig. S17, ESI†).

Synthesis of compound Co-1

Following a previously published procedure,[50,52,54] a mixture solution of **3** (466 mg, 0.740 mmol) in THF (80.00 mL) was treated with NaH (60% w/w, 90 mg, 2.2 mmol) at room temperature under an N_2 atmosphere. After 15 min, 1,3-dibromo-propane (0.75 mL, 7.4 mmol) was added to the resulting purple suspension and then the mixture was refluxed for 38 h. After the reaction was cooled to room temperature, it was quenched with a saturated aqueous solution of NH_4Cl and extracted with EtOAc. The organic phase was washed with water, dried over anhydrous

MgSO$_4$ and concentrated to dryness. The resulting crude product was purified by column chromatography [silica gel, 0.1% Et$_3$N in CH$_2$Cl$_2$/hexanes (1:1)] to afford a purple solid mixture containing **3** and the elimination product, exhibiting molecular peaks at m/z 750.735 and 669.718, respectively, in their MALDI-TOF mass spectra. Then, this mixture was re-dissolved in CHCl$_3$ (36.0 mL) and reacted with a solution of Co(OAc)$_2$·4H$_2$O (63 mg, 0.25 mmol) in MeOH (3.0 mL) at room temperature for 12 h. After removal of the solvent, the resulting crude was dissolved with CH$_2$Cl$_2$, and washed with water and then a saturated aqueous solution of NaHCO$_3$. The organic phase was dried over anhydrous MgSO$_4$ and concentrated to dryness. The crude product was purified by column chromatography [silica gel, 0.5% Et$_3$N in CH$_2$Cl$_2$/hexanes (1:1)] to afford a purple solid mixture containing **Co-3** and a metallated elimination product, showing molecular peaks at m/z 807.580 and 725.599, respectively, in the MALDI-TOF mass spectrum.

In another round-bottomed flask, a solution of **4**[50] (16 mg, 0.095 mmol) in anhydrous DMF (2.0 mL) under an N$_2$ atmosphere was cooled to 20 °C. Then, a reaction mixture of CsOH (16 mg, 0.095 mmol) in degassed MeOH (0.5 mL) was added dropwise and the reaction was continued at 20 °C for 1 h. Subsequently, a solution of the mixture containing **Co-3** in anhydrous DMF (3.0 mL) was added dropwise and the reaction mixture was stirred at room temperature for an additional 6 h. Then, the resulting mixture was diluted with CH$_2$Cl$_2$, washed with water, dried over anhydrous MgSO$_4$, and concentrated to dryness. The crude product was purified by column chromatography [silica gel, 0.5% Et$_3$N in CH$_2$Cl$_2$/hexanes (1:1)]. After washing with hexanes and MeOH under ultrasonic agitation, **Co-1** was obtained as a purple solid (7 mg, 1% from compound **2**). Due to its paramagnetic nature, the NMR data of **Co-1** could not be obtained. HR-ESI-MS m/z: [M]$^+$ calcd for C$_{57}$H$_{41}$CoN$_5$O$_2$S$_3$, 982.1754; found 982.1758; λ_{abs} (ε, [**Co-1**] = 6.68 μM) 432 (7.4 × 10^4), 550, 596 nm; λ_{em} (λ_{ex} = 432 nm, [**Co-1**] = 2.00 μM) 611, 656 nm.

Electropolymerization of Zn-1 and Co-1

The target polymers were obtained *via* electropolymerization on ITO-coated glass and carbon paper at room temperature by means of CV. The ITO-coated glass (~15 Ohm square^{-1}) and commercial carbon paper AvCarb® MGL190 (190 μm in thickness, porosity 78% and bulk density 0.44 g cm^{-3}) were purchased from Semiconductor Wafer and Fuel Cell Store, respectively. According to a previous study, the specific surface area of the carbon paper was 5.6 m^2 g^{-1}.[78] Cyclic voltammograms were recorded with a potentiostat/galvanostat at room temperature. A conventional three-electrode one-compartment system consisting of the ITO-coated glass or carbon paper as the WE, Pt plate as the CE, and Ag/AgCl QRE was used. The Ag/AgCl QRE was prepared using a previously reported method.[79] The ITO-coated glass was cut into 0.8 cm × 4.0 cm pieces, ultrasonically cleaned in isopropanol and acetone for 15 min each, and then rinsed with CH$_2$Cl$_2$, while the carbon paper was cut into 1.0 cm × 2.0 cm pieces and rinsed with acetone before use. Each monomer solution was prepared in

a 0.1 M TBAPF$_6$ solution in dry CH$_2$Cl$_2$ at a concentration of 0.25 mM, and degassed with N$_2$ for 15 min before the electropolymerization. A water cooling bath was used to avoid evaporation of the solvent. The potential between 0.36 V and 1.96 V or 2.06 V vs. NHE was swept at the scan rate of 50 mV s^{-1} with the number of the scanning cycles of 10. The polymers were coated on the ITO-coated glass and carbon paper on an area of 0.8 cm × 2.0 cm and 1.0 cm × 1.2 cm, respectively. Subsequently, the WE was removed from the solution and rinsed with CH$_2$Cl$_2$ to remove the remaining monomer. The E^0 of the Fc$^+$/Fc redox couple in 0.1 M TBAPF$_6$ solution in DMF was used for calibration of the Ag/AgCl QRE and for conversion to the NHE scale using the reference value of E^0(Fc$^+$/Fc) = 0.72 V vs. NHE in DMF.[56]

Electrochemical characterization of polymer films on substrates.

CV was used to investigate the electrochemical behavior of the **poly(Zn-1)**- and **poly(Co-1)**-modified ITO-coated glass and carbon paper in 0.1 M TBAPF$_6$ solution in DMF and one-compartment three-electrode electrochemical setup. The area of 0.8 cm × 1.5 cm and 1.0 cm × 1.0 cm of the polymer films on the ITO-coated glass and carbon paper, respectively, was dipped in the electrolyte solution. The Ag/AgCl QRE and Pt plate served as the RE and the CE, respectively. The cyclic voltammograms of these polymer-modified electrodes were recorded in the potential range of 0.36 V to 1.66 V vs. NHE at the scan rate of 50 mV s^{-1}. Prior to each CV measurement, N$_2$ was purged in the electrolyte solution for 15 min. All potentials against the Ag/AgCl QRE were calibrated with the Fc$^+$/Fc redox couple and converted to the NHE scale using the reference value of E^0(Fc$^+$/Fc) = 0.72 V vs. NHE in DMF.[56]

Determination of electrocatalytic activities of poly(Zn-1) and poly(Co-1) for the ECR of CO$_2$

The heterogeneous ECR of CO$_2$ under the catalysis of the target polymeric films was carried out in 0.5 M KHCO$_3$ aqueous solution at room temperature. The CV studies were performed in the three-electrode two-compartment setup consisting of cathodic and anodic chambers. The cathodic chamber contained **poly(Zn-1)** or **poly(Co-1)**/carbon paper and Ag/AgCl, 3 M KCl serving as the WE and RE, respectively. The area of 1.0 cm × 1.0 cm of the polymer films was dipped in the electrolyte solution. A Pt plate was used as the CE and placed in the anode chamber. Both chambers were separated from each other by a glass frit to prevent the reduction products generated at the cathode from getting oxidized at the anode. The potential between 0.00 V and −1.30 V vs. Ag/AgCl, 3 M KCl or −0.66 V vs. RHE was applied to the H-cell at a scan rate of 50 mV s^{-1} for 3 cycles. N$_2$ or CO$_2$ was purged in the 0.5 M KHCO$_3$ aqueous solutions for 20 min prior to each measurement, leading to electrolyte solutions with the measured pH values of 8.4 and 7.3, respectively. The potentials against Ag/AgCl, 3 M KCl were calibrated by the E^0 of potassium ferricyanide in 1 M KCl (aqueous solution) and converted to the RHE scale

using the following equation: $E_{vs. \text{RHE}} = E_{vs. \text{Ag/AgCl 3M KCl}} + 0.059\text{pH} + 0.21 \text{ V}$.[64]

The CPE experiments were conducted in the same setup as mentioned above. The constant potential at -0.66 V *vs.* RHE was applied for 1 or 6 h to the H-cell under CO_2-saturated conditions (pH = 7.3). The headspace gas (4 mL from total volume of 19.0 mL) was taken by a gas-tight syringe and a portion of this gas sample (2 mL) was analyzed using a Thermo Scientific Trace GC Ultra equipped with a thermal conductivity detector (TCD) for CO and H_2 production using He and N_2 as carrier gases, respectively. For the 1 h CPE, the product analysis was performed once when the reaction ran to completion, while CO_2 was continuously purged in the cathodic electrolyte at the flow rate of $5.0 \pm 0.5\%$ mL min^{-1} and the gas sample was collected for product analysis every 30 min in the 6 h experiment.

For liquid phase analysis, samples of the electrolysis solution (20 µL) were diluted with ultrapure water (1980 µL), filtered by a syringe filter and determined using a Thermo Scientific Dionex ICS-5000 ion chromatography (IC) system equipped with a suppressor-conductivity detector using gradient KOH as the eluent. The concentration of the KOH solution in ultrapure water was periodically programed by 10 mM KOH (0 to 7 min); 100 mM KOH (7 to 14 min); 10 mM KOH (14 to 27 min) at a constant temperature of 25 °C with the flow rate of 0.25 mL min^{-1}. For all the samples in these experiments, no significant amount of formate ions was detected.

Conflicts of interest

There are no conflicts to declare.

Acknowledgements

Notes and references

1 G. Mele, C. Annese, L. D'Accolti, A. De Riccardis, C. Fusco, L. Palmisano, A. Scarlino and G. Vasapollo, *Molecules*, 2015, **20**, 396–415.

2 D. M. D'Alessandro, B. Smit and J. R. Long, *Angew. Chem., Int. Ed.*, 2010, **49**, 6058–6082.

3 G. F. Manbeck and E. Fujita, *J. Porphyrins phthalocyanines*, 2015, **19**, 45–64.

4 D. H. Apaydin, S. Schlager, E. Portenkirchner and N. S. Sariciftci, *ChemPhysChem*, 2017, **18**, 3094–3116.

5 J. Hong, W. Zhang, J. Ren and R. Xu, *Anal. Methods*, 2013, **5**, 1086–1097.

6 D. T. Whipple and P. J. A. Kenis, *J. Phys. Chem. Lett.*, 2010, **1**, 3451–3458.

7 W. Zhang, Y. Hu, L. Ma, G. Zhu, Y. Wang, X. Xue, R. Chen, S. Yang and Z. Jin, *Adv. Sci.*, 2018, **5**, 1700275.

8 A. S. Agarwal, E. Rode, N. Sridhar and D. Hill, *Handbook of Climate Change Mitigation and Adaptation*, Springer International Publishing, 2015, pp. 1–40.

9 D. H. Apaydin, E. Tordin, E. Portenkirchner, G. Aufischer, S. Schlager, M. Weichselbaumer, K. Oppelt and N. S. Sariciftci, *ChemistrySelect*, 2016, **1**, 1156–1162.

10 M. A. Baldo, D. F. O'Brien, Y. You, A. Shoustikov, S. Sibley, M. E. Thompson and S. R. Forrest, *Nature*, 1998, **395**, 151–154.

11 R. C. Kwong, S. Sibley, T. Dubovoy, M. Baldo, S. R. Forrest and M. E. Thompson, *Chem. Mater.*, 1999, **11**, 3709–3713.

12 E. M. Gross, N. R. Armstrong and R. M. Wightman, *J. Electrochem. Soc.*, 2002, **149**, 137–142.

13 V. A. Montes, C. Pérez-Bolívar, N. Agarwal, J. Shinar and P. Anzenbacher, *J. Am. Chem. Soc.*, 2006, **128**, 12436–12438.

14 X. Wang, H. Wang, H. Yang, Y. He, L. Zhang, Y. Li and X. Li, *Macromolecules*, 2010, **43**, 709–715.

15 Y.-Y. Noh, J.-J. Kim, K. Yase and S. Nagamatsu, *Appl. Phys. Lett.*, 2003, **83**, 1243–1245.

16 P. B. Shea, J. Kanicki and N. Ono, *J. Appl. Phys.*, 2005, **98**, 014503.

17 X. Huang, C. Zhu, S. Zhang, W. Li, Y. Guo, X. Zhan, Y. Liu and Z. Bo, *Macromolecules*, 2008, **41**, 6895–6902.

18 P. Ma, Y. Chen, X. Cai, H. Wang, Y. Zhang, Y. Gao and J. Jiang, *Synth. Met.*, 2010, **160**, 510–515.

19 Y. Liu, N. Xiang, X. Feng, P. Shen, W. Zhou, C. Weng, B. Zhao and S. Tan, *Chem. Commun.*, 2009, 2499–2501.

20 A. Yella, H.-W. Lee, H. N. Tsao, C. Yi, A. K. Chandiran, M. K. Nazeeruddin, E. W.-G. Diau, C.-Y. Yeh, S. M. Zakeeruddin and M. Grätzel, *Science*, 2011, **334**, 629–634.

21 K. Ladomenou, V. Nikolaou, G. Charalambidis and A. G. Coutsolelos, *Dalton Trans.*, 2016, **45**, 1111–1126.

22 N. V. Krishna, J. V. S. Krishna, S. P. Singh, L. Giribabu, L. Han, I. Bedja, R. K. Gupta and A. Islam, *J. Phys. Chem. C*, 2017, **121**, 6464–6477.

23 K. Prakash, S. Manchanda, V. Sudhakar, N. Sharma, M. Sankar and K. Krishnamoorthy, *Dyes Pigm.*, 2017, **147**, 56–66.

24 H. Song, X. Li, H. Ågren and Y. Xie, *Dyes Pigm.*, 2017, **137**, 421–429.

25 J. Hatano, N. Obata, S. Yamaguchi, T. Yasuda and Y. Matsuo, *J. Mater. Chem.*, 2012, **22**, 19258–19263.

26 W. Keawsongsaeng, J. Gasiorowski, P. Denk, K. Oppelt, D. H. Apaydin, R. Rojanathanes, K. Hingerl, M. Scharber, N. S. Sariciftci and P. Thamyongkit, *Adv. Energy Mater.*, 2016, **6**, 1600957.

27 F.-C. Hsu, J.-L. Chen, C. Kashi, P.-W. Tsao, C.-Y. Yeh, T.-Y. Lin and Y.-F. Chen, *J. Phys. Chem. C*, 2017, **121**, 20084–20092.

28 A. Fukatsu, M. Kondo, Y. Okabe and S. Masaoka, *J. Photochem. Photobiol., A*, 2015, **313**, 143–148.

29 B. Mondal, A. Rana, P. Sen and A. Dey, *J. Am. Chem. Soc.*, 2015, **137**, 11214–11217.

30 J. Shen, R. Kortlever, R. Kas, Y. Y. Birdja, O. Diaz-Morales, Y. Kwon, I. Ledezma-Yanez, K. J. P. Schouten, G. Mul and M. T. M. Koper, *Nat. Commun.*, 2015, **6**, 8177.

31 X.-M. Hu, Z. Salmi, M. Lillethorup, E. B. Pedersen, M. Robert, S. U. Pedersen, T. Skrydstrup and K. Daasbjerg, *Chem. Commun.*, 2016, **52**, 5864–5867.

32 J. E. Pander, A. J. Fogg and A. B. Bocarsly, *ChemCatChem*, 2016, **8**, 3536–3545.

33 Z. Weng, J. Jiang, Y. Wu, Z. Wu, X. Guo, K. L. Materna, W. Liu, V. S. Batista, G. W. Brudvig and H. Wang, *J. Am. Chem. Soc.*, 2016, **138**, 8076–8079.

34 Y. Wu, J. Jiang, Z. Weng, M. Wang, D. L. J. Broere, Y. Zhong, G. W. Brudvig, Z. Feng and H. Wang, *ACS Cent. Sci.*, 2017, **3**, 847–852.

35 B. Zhao, H. Lei, N. Wang, G. Xu, W. Zhang and R. Cao, *Chem. – Eur. J.*, 2020, **26**, 4007–4012.

36 K. Guo, X. Li, H. Lei, W. Zhang and R. Cao, *ChemCatChem*, 2020, **12**, 1591–1595.

37 L. Lin, C. Hou, X. Zhang, Y. Wang, Y. Chen and T. He, *Appl. Catal., B*, 2018, **221**, 312–319.

38 H. Chen, J. Zeng, F. Deng, X. Luo, Z. Lei and H. Li, *J. Polym. Res.*, 2012, **19**, 9880.

39 B. Kolodziejczyk, D. Mayevsky and B. Winther-Jensen, *RSC Adv.*, 2013, **3**, 4568–4573.

40 A. J. Heeger, *Rev. Mod. Phys.*, 2001, **73**, 681–700.

41 M. Schaferling and P. Bauerle, *J. Mater. Chem.*, 2004, **14**, 1132–1141.

42 G. E. Collis, W. M. Campbell, D. L. Officer and A. K. Burrell, *Org. Biomol. Chem.*, 2005, **3**, 2075–2084.

43 N. Xiang, Y. Liu, W. Zhou, H. Huang, X. Guo, Z. Tan, B. Zhao, P. Shen and S. Tan, *Eur. Polym. J.*, 2010, **46**, 1084–1092.

44 X. Luo, F. Wu, H. Xiao, H. Guo, Y. Liu and S. Tan, *Synth. Met.*, 2017, **223**, 205–211.

45 K. Takechi, T. Shiga, T. Motohiro, T. Akiyama, S. Yamada, H. Nakayama and K. Kohama, *Sol. Energy Mater. Sol. Cells*, 2006, **90**, 1322–1330.

46 C. D. Windle and R. N. Perutz, *Coord. Chem. Rev.*, 2012, **256**, 2562–2570.

47 J. Park, H. Lee, Y. E. Bae, K. C. Park, H. Ji, N. C. Jeong, M. H. Lee, O. J. Kwon and C. Y. Lee, *ACS Appl. Mater. Interfaces*, 2017, **9**, 28758–28765.

48 J. Roncali, *Chem. Rev.*, 1992, **92**, 711–738.

49 M. J. Zöllner, E. Becker, U. Jahn, W. Kowalsky and H. H. Johannes, *Eur. J. Org. Chem.*, 2010, 4426–4435.

50 B. Jousselme, P. Blanchard, M. Ocafrain, M. Allain, E. Levillain and J. Roncali, *J. Mater. Chem.*, 2004, **14**, 421–427.

51 G.-P. Yan, D. Bischa and S. E. Bottle, *Free Radical Biol. Med.*, 2007, **43**, 111–116.

52 R. M. Schelkun, P.-W. Yuen, K. Serpa, L. T. Meltzer, L. D. Wise, E. R. Whittemore and R. M. Woodward, *J. Med. Chem.*, 2000, **43**, 1892–1897.

53 J. Jiao, P. Thamyongkit, I. Schmidt, J. S. Lindsey and D. F. Bocian, *J. Phys. Chem. C*, 2007, **111**, 12693–12704.

54 Y. Xie, F. Zhang, P. Liu, F. Hao and H. A. Luo, *Can. J. Chem.*, 2014, **92**, 49–53.

55 K. Sakai, S. Iwamura, R. Sumida, I. Ogino and S. R. Mukai, *ACS Omega*, 2018, **3**, 691–697.

56 T. J. Smith and K. J. Stevenson, *Handbook of Electrochemistry*, ed. C. G. Zoski, Elsevier, Amsterdam, 2007, pp. 73–110.

57 T. Shimidzu, H. Segawa, F. Wu and N. Nakayama, *J. Photochem. Photobiol., A*, 1995, **92**, 121–127.

58 G. Li, S. Bhosale, S. Tao, R. Guo, S. Bhosale, F. Li, Y. Zhang, T. Wang and J.-H. Fuhrhop, *Polymer*, 2005, **46**, 5299–5307.

59 G. Ramachandraiah, F. Bedioui, J. Devynck, M. Serrar and C. Bied-Charreton, *J. Electroanal. Chem.*, 1991, **319**, 395–402.

60 E. Balasubramaniam, G. Ramachandraiah, P. Natarajan, C. Bied-Charreton, J. Devynck and F. Bedioui, *J. Mater. Chem.*, 1995, **5**, 625–629.

61 B. Jousselme, P. Blanchard, E. Levillain, R. de Bettignies and J. Roncali, *Macromolecules*, 2003, **36**, 3020–3025.

62 C. Matlachowski and M. Schwalbe, *Dalton Trans.*, 2015, **44**, 6480–6489.

63 R. Borjas and D. A. Buttry, *Chem. Mater.*, 1991, **3**, 872–878.

64 P. D. Tran, S. Y. Chiam, P. P. Boix, Y. Ren, S. S. Pramana, J. Fize, V. Artero and J. Barber, *Energy Environ. Sci.*, 2013, **6**, 2452–2459.

65 J. Jiang, A. J. Matula, J. R. Swierk, N. Romano, Y. Wu, V. S. Batista, R. H. Crabtree, J. S. Lindsey, H. Wang and G. W. Brudvig, *ACS Catal.*, 2018, **8**, 10131–10136.

66 K. Jiang, S. Siahrostami, T. Zheng, Y. Hu, S. Hwang, E. Stavitski, Y. Peng, J. Dynes, M. Gangisetty, D. Su, K. Attenkofer and H. Wang, *Energy Environ. Sci.*, 2018, **11**, 893–903.

67 C. S. Chen, A. D. Handoko, J. H. Wan, L. Ma, D. Ren and B. S. Yeo, *Catal. Sci. Technol.*, 2015, **5**, 161–168.

68 J. G. Goodwin Jr., S. Kim and W. D. Rhodes, in *Catalysis*, ed. J. J. Spivey and G. W. Roberts, RSC, 2004, vol. 17, pp. 320–348.

69 X.-M. Hu, Z. Salmi, M. Lillethorup, E. B. Pedersen, M. Robert, S. U. Pedersen, T. Skrydstrup and K. Daasbjerg, *Chem. Commun.*, 2016, **52**, 5864–5867.

70 M. Hammouche, D. Lexa, M. Momenteau and J.-M. Savéant, *J. Am. Chem. Soc.*, 1991, **113**, 8455–8466.

71 J. G. Lanese and G. S. Wilson, *J. Electrochem. Soc.*, 1972, **119**, 1039–1043.

72 G. Zhao, K. Rui, S. X. Dou and W. Sun, *Adv. Funct. Mater.*, 2018, **28**, 1803291.

73 X. M. Hu, M. H. Rønne, S. U. Pedersen, T. Skrydstrup and K. Daasbjerg, *Angew. Chem., Int. Ed.*, 2017, **56**, 6468–6472.

74 C. S. Diercks, S. Lin, N. Kornienko, E. A. Kapustin, E. M. Nichols, C. Zhu, Y. Zhao, C. J. Chang and O. M. Yaghi, *J. Am. Chem. Soc.*, 2018, **140**, 1116–1122.

75 S. Lin, C. S. Diercks, Y.-B. Zhang, N. Kornienko, E. M. Nichols, Y. Zhao, A. R. Paris, D. Kim, P. O. M. Yaghi and C. J. Chang, *Science*, 2015, **349**, 1208–1213.

76 N. Corbin, J. Zeng, K. Williams and K. Manthiram, *Nano Res.*, 2019, **12**, 2093–2125.

77 J. Shen, M. J. Kolb, A. J. Göttle and M. T. M. Koper, *J. Phys. Chem. C*, 2016, **120**, 15714–15721.

78 T. A. Ha, C. Pozo-Gonzalo, K. Nairn, D. R. MacFarlane, M. Forsyth and P. C. Howlett, *Sci. Rep.*, 2020, **10**, 7123.

79 A. W. Hassel, K. Fushimi and M. Seo, *Electrochem. Commun.*, 1999, **1**, 180–183.